The influence of a cyclic loading history on soil-geogrid interaction under pullout condition

THE INFLUENCE OF A CYCLIC LOADING HISTORY ON SOIL-GEOGRID INTERACTION UNDER PULLOUT CONDITION

G. Cardile[1], M. Pisano[2] and N. Moraci[3]

1 Assistant Professor of Geotechnical Engineering, Ph.D. — *Mediterranea* University of Reggio Calabria, Department of Civil Engineering, Energy, Environment and Materials (DICEAM), Italy- Telephone: +39 0965 169 2213; Telefax: +39 0965 1692201, e-mail: giuseppe.cardile@unirc.it (corresponding author)

2 Research assistant in Geotechnical Engineering, Ph.D. — *Mediterranea* University of Reggio Calabria, Department of Civil Engineering, Energy, Environment and Materials (DICEAM), Italy- Telephone: +39 0965 169 2223; Telefax: +39 0965 1692201, e-mail: marilene.pisano@unirc.it

3 Full Professor of Geotechnical Engineering, Ph.D. — *Mediterranea* University of Reggio Calabria, Department of Civil Engineering, Energy, Environment and Materials (DICEAM), Italy- Telephone: +39 0965 169 2263; Telefax: +39 0965 1692201, e-mail: nicola.moraci@unirc.it

ABSTRACT

The knowledge of soil-geosynthetic interface behaviour is a key point in the design of geosynthetic-reinforced soil structures. The pullout ultimate limit state can be reproduced conveniently by means of pullout tests performed with large-size laboratory apparatuses, which allow studying the interaction mechanisms that develop in the anchorage zone. During the service life of geosynthetic-reinforced soil structures, reinforcements may be subjected to long-term cyclic vehicular loads or short-term seismic loads in addition to dead loadings, such as the structure's self-weight and other sustained loads. In order to study the influence of a cyclic loading history (a sinusoidal function with fixed amplitude *A*, number of cycles *N* and frequency *f*) on the post-cyclic peak pullout resistance, the writers carried out a series of multi-stage pullout tests on a high density polyethylene extruded uniaxial geogrid embedded in a compacted granular soil for different vertical effective stress σ'_v values. Moreover, the stability of the soil-geosynthetic interface from a point of view linked to the cyclic loading application has also been investigated. Test results showed that the design pullout resistance parameters are affected by the applied cyclic loading history for specific combined conditions (*A*, *N* and σ'_v) and it should be taken into account for designing geosynthetic reinforced soil structures.

KEYWORDS: geosynthetics, geogrid, pullout, cyclic loading, soil-reinforcement interface, multi-stage test, residual strain, design parameters, apparent coefficient of friction, viscous properties.

1 INTRODUCTION

Different approaches can be used to study the seismic behaviour of geosynthetic-reinforced soil (GRS) structures, ranging from empirical observations of damages caused on GRS works by seismic events (Carrubba and Colonna, 2000; Huang et al., 2003; Koseki et al., 2006; Koseki et al., 2009; Ling and Leshchinsky, 2005; Ling et al., 2001; Tatsuoka et al., 1995, 1997; Wartman et al., 2006; White and Holtz, 1994) to the results' interpretation of tests carried out on full-scale or reduced-scale physical models (Capilleri et al., 2019; El-Emam and Bathurst, 2004; El-Emam and Bathurst, 2005; Izawa et al., 2004; Ling et al., 2005; Matsuo et al., 1998; Nova-Roessig and Sitar, 2006; Sabermahani et al., 2009; Watanabe et al., 2003), up to theoretical studies such as *pseudo-static analyses* (Bathurst and Cai, 1995; Biondi et al., 2013; Michalowski, 1998; Motta, 1996; Nouri et al., 2006), *seismic displacement analyses* (Ausilio et al., 2000; Cai and Bathurst, 1996a, b; Di Filippo et al., 2019; Gaudio et al., 2018; Ling et al., 1997; Michalowski and You, 2000; Paulsen and Kramer, 2004) and *dynamic numerical methods* (Hatami and Bathurst, 2000; Lee et al., 2010; Ling et al., 2004).

One of the parameters necessary to design GRS works by using the pseudo-static approach is the apparent coefficient of friction between soil and geosynthetic, which allows determining the reinforcement length and consequently the reinforced block size (Abramento, 1995; Carbone et al., 2015; Jewell, 1990; Leshchinsky, 2009; Leshchinsky et al., 2014; Leshchinsky et al., 1995; Moraci and Cardile, 2008; Moraci et al., 2014; Moraci and Recalcati, 2006; Pavanello et al., 2018).

The seismic displacement analyses are performance-based approaches that originate from the Newmark's sliding block method (Newmark, 1965), assuming that the soil mass moves as a rigid block along a potential sliding surface, with permanent displacements occurring when the forces acting on it exceed the available shear resistance. Whenever the ground acceleration overcomes the critical acceleration, the rigid block's permanent displacement increases and it can be considered as a measure of the possible damage caused by an earthquake. The friction interaction coefficient between soil and reinforcement is required also in these cases.

The dynamic analysis uses numerical methods such as finite element, finite difference and coupled finite element-discrete element methods, which need as input constitutive models capable to reproduce the stress-strain relationships for soil, geosynthetics and soil-reinforcement interfaces in the best way possible so as to provide accurate results. Therefore, comprehension of the soil-geosynthetic interface behaviour is extremely important whichever seismic method is chosen to design GRS structures. For this purpose, it is necessary to analyse the soil-geosynthetic interaction in terms of pullout resistance and displacement behaviour by using pullout tests under cyclic loading conditions as the more suitable tool. As things stand, few researches studied these aspects on different geosynthetics-granular soil interfaces generally subject to cyclic loading at frequencies up to 0.5 Hz (Min et al., 1995; Moraci and Cardile, 2009, 2012; Nayeri and Fakharian, 2009; Nernheim, 2005; Raju and Fannin, 1997; Razzazan et al., 2018; Yasuda et al., 1992). In this context, the paper aims to expand knowledge of the cyclic and post-cyclic pullout behaviour of a high density polyethylene (HDPE) extruded uniaxial geogrid embedded in a compacted granular soil subject to cyclic pullout loading with a higher frequency (f =1 Hz), more representative of long-term vehicular loads or short-term seismic loads, varying the cyclic load amplitude and the vertical effective stress. To take into account cyclic or dynamic loads potentially acting on GRS structures' reinforcements in addition to sustained loadings, the pullout tests were carried out using a multi-stage procedure. The influences of cyclic tensile loading amplitude A, number of cycles N and vertical effective stress σ'_v on the parameters obtained during hysteresis loops have been analysed in depth. Moreover, the difference between post-cyclic and static peak pullout resistances has also been investigated by comparing pullout curves for the multi-stage tests and those for the corresponding tests at constant rate of displacement.

2 EXPERIMENTAL STUDY

2.1 Apparatus

The test apparatus used in the research (Cardile et al., 2016a; Moraci and Recalcati, 2006) consists of different components (Figure 1a, b, c):

i) a pullout steel box having large dimensions (1700x600x680 mm) and walls covered with Teflon films to avoid friction effects;

ii) a rubber flexible membrane filled with air for the application of vertical loads;
iii) a hydraulic actuator for displacement- or load-controlled pullout testing for the application of horizontal loads;
iv) a clamping system inside the box to maintain the reinforcement specimen always confined for the whole duration of the test;
v) a pair of metal sleeves at the front wall to avoid its stiffness effects on results;
vi) a load cell for measuring the pullout force; and
vii) six linear variable displacement transducers (LVDT) connected to six different points of the reinforcement's specimen by means of inextensible steel wires to measure the specimen's displacements.

Unlike the apparatus used in previous researches, the new actuator is able to simulate pullout cyclic loadings that can reach high frequencies (up to 4 Hz).

2.2 Test materials

The soil used in this research is a uniform medium sand classified as SP and A-3 according to USCS (ASTM D2487, 2017) and UNI EN ISO 14688-1 (2018) classification systems respectively, with grain shape ranging from sub-rounded to rounded, uniformity coefficient (U) equal to 1.96, and average grain size (D_{50}) equal to 0.32 mm. The compaction of soil inside the pullout box was carried out until reaching a dry unit weight value equal to 95% of the maximum dry unit weight (γ_{dmax} = 16.24 kN/m^3, at an optimum water content w_{opt} = 13.5%) obtained by AASHTO T 99 (2015) Standard Proctor compaction tests (ASTM D698-12e2, 2012; UNI EN ISO 13286-2, 2010). Direct shear tests, performed at γ_d = 95% γ_{dmax}, yielded values of the soil peak shear-strength angle ϕ'_P from 48° (for σ'_v = 10 kPa) to 42° (for σ'_v = 100 kPa). The soil shear-strength angle at constant volume ϕ'_{CV} was equal to 34° (Moraci and Recalcati, 2006).

The geosynthetic used in the pullout tests is an HDPE uniaxial extruded geogrid. Its mechanical behaviour was investigated by means of wide-width tensile tests (Cardile et al., 2016b; Cardile et al., 2017b) in the standard atmosphere for testing (20±2°C at 65+5% RH) at constant strain rate (CSR) equal to 20% per minute, using index test procedures (ISO 10319:2015). Additional tensile tests at CSR equal to ε'=0.2% per minute were also carried out to make comparison with the rate used in pullout tests carried out at constant rate of displacement. Table 1 lists the tensile test results at constant strain rates equal to 20% and 0.2% per minute.

2.3 Test procedure

The multi-stage pullout tests were performed on geogrid specimens 1.20 m long, at different vertical effective stresses (σ'_v = 10, 25, 50, 100 kPa), by using a multi-stage procedure (MS) consisting of three steps (Moraci and Cardile, 2009, 2012):

• a displacement-controlled stage at constant rate of displacement (CRD) equal to 1 mm per minute, reaching a fixed pullout load P_i;

• a load-controlled cyclic stage using a sinusoidal function, with a fixed tensile loading amplitude A and frequency f=1 Hz, for N=1000 cycles in total;

• a post-cyclic stage that is a displacement-controlled stage at CRD=1 mm per minute once again, until a maximum horizontal displacement equal to 100 mm, the specimen pullout or its rupture was reached.

Both P_i and A were chosen as a percentage of P_R that is the peak pullout resistance (per unit width) obtained by pullout tests under static conditions, carried out at the same confining pressure and CRD=1 mm per min. Specifically, $P_i \approx 35\%\ P_R$ was adopted for the first one since it could be considered as an upper bound value (taking into account surcharge, geometry, partial coefficients to be used for the reduction of the interface parameters according to several international recommendations, etc.) for those representative of GRS structures' design. Moreover, in order to investigate the influence in changing the cyclic loading amplitude, two different A values ($A \approx 30\%\ P_R$ and $A \approx 45\%\ P_R$) were chosen for the maximum loading level falling into the range between P_i and P_R.

Table 2 lists the MS pullout test program, highlighting that the actually-made cycles were lower than the planned ones for the higher applied amplitude ($A \approx 45\%\ P_R$) at $\sigma'_v < 100$ kPa due to the achievement of the clamp maximum displacement allowed by this apparatus.

3 ANALYSIS OF TEST RESULTS

3.1 Cyclic stability of soil-geogrid interface

Accumulation of permanent strains, which occurs cycle by cycle under application of non-zero mean tensile stress (ratcheting), is observed on both soil and geosynthetics when a cyclic load is applied (Alonso-Marroquín and Herrmann, 2004; Calvetti and di Prisco, 2010; Cardile et al., 2016b; Cardile et al., 2017b; Kongkitkul et al., 2004; Ling et al., 1998; Vieira and Lopes, 2013). Likewise wide-width cyclic tensile tests, the application of cyclic pullout loads involves the development of hysteresis loops during the cyclic stage.

A cyclically stable behaviour of the polymeric reinforcement obtained by means of wide-width cyclic tensile tests (that is, increments of residual strain decrease with increasing number of loading cycles, Cardile et. al, 2017b) is not sufficient to assure a cyclically stable pullout behaviour of the interface soil-reinforcement since the cyclic loading entails geogrid's deformation as well as its pullout from the soil.

In order to analyse these points, the parameters obtained for each load–unload cycle are listed separately depending on the reference plane. Specifically, with regard to the P-δ plane (pullout load versus displacement of the first confined section of specimen) they are (Figure 2a):

- Cyclic displacement's increment measured at the first confined section of specimen (the specimen head attached to the clamp) and reached during each cyclic loading, $\Delta\delta^{h}_{part,i}$;
- Cumulative cyclic displacement of the specimen's first confined section, $\Delta\delta^{h}_{i} = \sum_{i=1}^{N} \Delta\delta^{h}_{part,i}$;
- Cyclic displacement's increment measured at the rear end of the specimen (the last transverse rib) and reached during each cyclic loading, $\Delta\delta^{e}_{part,i}$;
- Cumulative cyclic displacement of the specimen's rear end, $\Delta\delta^{e}_{i} = \sum_{i=1}^{N} \Delta\delta^{e}_{part,i}$.

Regarding the P-ε plane (pullout load versus pullout average strain), the parameters obtained are (Figure 2b):

- Residual strains caused by cyclic loading, ε_r, i.e. when the cyclic loading returns to the value of the fixed pullout load P_i.

For each of these parameters, the influence of tensile loading amplitude A, number of cycles N and vertical effective stress σ'_v has been investigated.

In order to analyse the behaviour at the soil-reinforcement interface, the conceptual model proposed by Moraci and Cardile (2012) has been used by applying a double-graph that shows the relationship between the number of cycles *N* and $\Delta\delta^h$ on the top part, and between $\Delta\delta^e$ and $\Delta\delta^h$ on the bottom one (Figure 3, Figure 4 and Figure 5). The graphic representations on the top part (Figure 3a, Figure 4a and Figure 5a) allow understanding when the behaviour of soil-reinforcement interface is stable/unstable from a point of view linked to the cyclic loadings application. For a fixed cyclic load history, the cumulative cyclic displacement of the specimen's first confined section is connected both to the residual strains of the geogrid, which occur cycle by cycle under application of cyclic pullout stress, and to the progressive mobilisation of the interaction mechanisms along the specimen that could induce pullout failure.

The writers define that the soil-reinforcement interface is cyclically stable when a progressive stabilisation of the interface response is observed. Specifically, this means that the curve $N-\Delta\delta^h$ is concave upward and the cyclic displacement's increments $\Delta\delta^h_{part,i}$ decrease with increasing numbers of cycles: the displacement accumulation rate decreases with increasing *N*. Nevertheless, it is important to observe that such a cyclically stable condition could be engineeringly unacceptable if the cumulative displacements during the cyclic stage are larger than the allowable displacement for the serviceability limit state.

On the contrary, the soil-geogrid interface cyclic behaviour is cyclically unstable when the cyclic displacement's increments $\Delta\delta^h_{part,i}$ become constant or start to increase with increasing numbers of cycles. In the last case, the curve $N-\Delta\delta^h$ has an inflection point becoming concave downward that is, the displacement accumulation rate increases with increasing *N*, potentially precipitating the achievement of the reinforcement's limit state of failure due to insufficient interaction resistance under pullout conditions between soil and the reinforcement.

Regarding graphics on the bottom part (Figure 3b, Figure 4b and Figure 5b), they allow defining more in detail when the soil-geogrid interface approaches the critical condition of pullout failure during the cyclic phase, or rather when the reinforcement is in the:

- i) load transfer phase. During this phase the active length, that is the portion of the geogrid specimen on which the mobilisation of interaction mechanisms withstands the applied load (Cardile et al., 2016a), increases with the pullout force until this force reaches a limit value that causes the movement of the last transversal bar;
- ii) pullout phase. During this phase the rear end of the geogrid begins to move and the active length coincides with the entire length of the specimen plus its elongation;
- iii) pullout limit state. This condition happens when the displacement increments of all specimen points are the same (geogrid stops to deform).

Specifically, the reinforcement is in the load transfer phase when the curve $\Delta\boldsymbol{\delta}^{e}-\Delta\boldsymbol{\delta}^{h}$ evolves in parallel along the $\Delta\boldsymbol{\delta}^{h}$ x-axis for all cycles since the specimen's rear end is immobile. On the contrary, the reinforcement is in the pullout phase when the curve evolves inside the $\Delta\boldsymbol{\delta}^{e}-\Delta\boldsymbol{\delta}^{h}$ admissible area with cyclic displacement's increments of the specimen's rear end that are lower than the corresponding cyclic displacement's increment of the specimen's first confined section for all cycles. Finally, the reinforcement is in the pullout limit state when the curve $\Delta\boldsymbol{\delta}^{e}-\Delta\boldsymbol{\delta}^{h}$ becomes parallel with the boundary line between the admissible and inadmissible areas (the displacement's increment of geogrid's head is equal to the displacement's increment measured at the rear end for all the next cycles).

3.1.1 Effect of cyclic loading amplitude

In order to study the influence of loading amplitude A, the double-graph results of MS pullout tests carried out with two different loading amplitudes ($A \approx 30\%\ P_R$, $45\%\ P_R$) at the equal value of $P_i \approx 35\%\ P_R$ are plotted in Figure 3a,b and Figure 4a,b for $\sigma'_v = 50$ kPa and $\sigma'_v = 100$ kPa respectively; the results are representative of all the cases observed in the research.

In Figure 3a ($\sigma'_v = 50$ kPa), when $A \approx 30\%\ P_R$ it is possible to observe a cyclically stable behaviour of the soil-reinforcement interface during all the cyclic stage since the displacement accumulation rate decreases with increasing numbers of cycles. Referring to the results obtained with $A \approx 45\%\ P_R$, a cyclically unstable behaviour can be observed since there is an inflection point after a certain number of cycles and $\Delta\boldsymbol{\delta}^{h}_{part,i}$ starts to increase with increasing N (the displacement accumulation rate increases). With regard to the pullout condition, Figure 3b shows that when $A \approx 30\%\ P_R$ the $\Delta\boldsymbol{\delta}^{e} - \Delta\boldsymbol{\delta}^{h}$ curve evolves inside the admissible area but not in parallel with the boundary line (that is, the cyclic displacement's increment measured at the rear end is lower than the cyclic displacement's increment of the geogrid's head for all cycles), entailing that even the last transversal rib moved; therefore, the geogrid reached the pullout phase. Instead, when $A \approx 45\%\ P_R$, an unstable pullout behaviour arises as the $\Delta\boldsymbol{\delta}^{e} - \Delta\boldsymbol{\delta}^{h}$ curve becomes parallel with the boundary line after a certain number of cycles and pullout failure occurs ($\Delta\boldsymbol{\delta}^{e}_{part} = \Delta\boldsymbol{\delta}^{h}_{part}$).

For soil-geogrid interface tested at $\sigma'_v = 100$ kPa, a cyclically stable behaviour is noticed for both cyclic amplitudes (Figure 4a); specifically, $\Delta\boldsymbol{\delta}^{h}$ tends to settle towards a constant value with increasing numbers of cycles. Instead, the behaviour in terms of pullout condition is different, in fact while the geogrid is in the pullout phase when $A \approx 45\%\ P_R$, it is still in the load transfer phase when $A \approx 30\%\ P_R$ (Figure 4b) since the curve evolves in parallel along the $\Delta\delta^h$ x-axis for all cycles ($\Delta\delta^e = 0$).

Therefore, with regard to the loading amplitude influence it is possible to state that, N being equal, the slope of $N - \Delta\delta^h$ decreases with increasing loading amplitude: for cyclically stable interfaces, the ideal condition of $\Delta\delta^h$ being constant (the displacement accumulation rate is null) is reached for a number of cycles gradually decreasing with decreasing applied loading amplitude, while for cyclically unstable interfaces it is reasonable to expect that the number of cycles at which the displacement accumulation rate becomes constant, or a change in the direction of curvature occurs, decreases with increasing loading amplitude. In other words, the cyclic pullout behaviour of the soil-geogrid interface starts getting worse with increasing cyclic loading amplitude.

3.1.2 The role of vertical effective stresses

To evaluate the influence of the vertical effective stress σ'_v applied to the soil-geogrid interface, the strain behaviour has been investigated analysing MS pullout tests carried out with loading amplitude $A \approx 45\%\ P_R$ (the MS pullout tests at $A \approx 30\%\ P_R$ are omitted as they showed a similar behaviour). By observing the top part of Figure 5, the only cyclically stable behaviour is obtained for $\sigma'_v = 100$ kPa. For all the other vertical effective stresses applied, when the inflection point arises the cyclic displacement's increment of the specimen's head starts to increase until pullout failure.

On the bottom part of Figure 5 the relationship between the cumulative cyclic displacements of the specimen's first confined section, $\Delta\delta^h$, and the cumulative cyclic displacements of the specimen's rear end, $\Delta\delta^e$, shows an unstable behaviour in terms of pullout condition for σ'_v = 10, 25 and 50 kPa since their representative curves become parallel with the boundary line between the admissible and inadmissible areas for a number of cycles that increases with increasing σ'_v. When σ'_v = 100 kPa the interface is still in the pullout phase. Therefore, it is possible to observe that the increase of the vertical effective stress σ'_v plays a clear stabilising role.

3.2 Residual strains and comparison with in-air results

Another important parameter to study the cyclic strain behaviour of the soil-geosynthetic interface is the residual strain ε_r, defined as the cumulative deformation mobilised in the specimen at the end of each corresponding cycle (when the cyclic loading returns to P_i), in agreement with Figure 2b. This parameter allows taking into account the confined stiffness of the geogrid, which exhibits a different response depending on geogrid's geometry, soil type, initial stress state and cyclic loading history.

The influence of the vertical effective stress and cyclic loading amplitude is showed in Figure 6a, where the residual strain (evaluated for the entire length of the geogrid, i.e. *apparent strain*) reached at N = 10 is plotted versus the vertical effective stress for tests performed at $A \approx 30\%\ P_R$ and $A \approx 45\%\ P_R$. The results highlight that the residual strain increases non-linearly with increasing vertical effective stress and, σ'_v being equal, it increases with increasing loading amplitude. The choice to plot the residual strains at cycle N = 10 is because tests with $A \approx 45\%\ P_R$ do not complete all cycles since pullout occurred and the clamp reached the maximum displacement allowed by the apparatus, as it can be observed in Figure 6b. The latter graph displays the residual strain ε_r for varying numbers of cycles on a logarithmic scale, for tests carried out with loading amplitude $A \approx 45\%\ P_R$ at different vertical effective stress values. It is possible to observe that the residual strain ε_r increases with increasing numbers of cycles and, N being equal, increases with increasing vertical effective stress. Moreover, the number of cycles where the interface exhibits an instable behaviour decreases with decreasing σ'_v (N = 158, 148, 20 for σ'_v = 50, 25, 10 kPa respectively).

Kongkitkul et al. (2004) stated that, for the geosynthetic reinforcement types examined by them (such as the HDPE geogrids of this research), the residual strain developed during a certain cyclic loading history is basically due to the loading rate effects caused by the intrinsic viscous properties of the material (therefore, it is controlled by the total period of cyclic loading). The nature of this residual strain is essentially the same as for creep strain developing under an equivalent sustained load. The current research allows studying how the soil confinement affects geogrids strain. Figure 6b points out that for σ'_v ranging from 10 to 50 kPa the ε_r - N curve deviates from linearity in the semi-logarithmic graph: the strain accumulation rate starts to increase in correspondence with a certain number of cycles that increases with increasing vertical effective stress, highlighting viscous effects similar to the "tertiary creep" phenomenon observed in tensile creep tests, that imply a possible tensile rupture of the reinforcement in case pullout failure does not occur first, such as in this research. Instead, when σ'_v = 100 kPa the change in ε_r trend is missing since the soil confinement employs a positive effect (Bathurst et al., 2004; Carrubba et al., 2000; Franca and Bueno, 2011; Kongkitkul et al., 2007a, b; Tatsuoka, 2008) increasing the range of numbers of cycles where the strain accumulation rate remains constant (as for the secondary creep phase under sustained tensile loads).

Afterwards, by considering the soil-geogrid interface tested at σ'_v =100 kPa and $A \approx 30\%\ P_R$, $45\%\ P_R$ for which a progressive stabilisation of the interface response has been observed, a comparison between their results and those obtained by wide-width tensile multi-stage tests (Cardile et al., 2017b) has been made. In-air tensile tests procedure was similar to the pullout one, with three different stages (two displacement-controlled tensile stages separated by one load-controlled cyclic stage) at the same test conditions (in terms of rate of displacement, P_i, A, N and f). It is more proper to analyse residual strains taking into account the progressive failure mechanisms related to the extensibility of the reinforcement under soil confinement; as a matter of fact, by evaluating individually the residual strains of geogrid's different sections (from a transversal rib to another), the results change remarkably. Figure 7 shows the residual strains evaluated in the cyclic phase of the MS pullout tests for (i) the entire length of the geogrid (residual apparent strains), and (ii) the geogrid's monitored portion closer to its head for varying number of loading cycles at σ'_v = 100 kPa, $A \approx 30\%\ P_R$ (Figure 7a) and σ'_v = 100 kPa, $A \approx 45\%\ P_R$ (Figure 7b), and the comparison with the corresponding wide-width MS tensile test (Cardile et al., 2017b). This comparison is possible only because the high soil confinement (100 kPa) is preventing the pullout failure, allowing the increase of the applied tensile load. The tensile load applied at the geogrid's head decreases along the specimen until it becomes null (the interaction mechanisms are progressively mobilised on the active length).

The shape of the distribution curve representing the tensile stresses along the interface can be very complex, depending on: (i) boundary conditions, (ii) soil mechanical characteristics, and (iii) structural, geometrical and mechanical characteristics of the reinforcement (Bathurst and Ezzein, 2017; Cardile et al., 2014; Cardile et al., 2016a; Moraci et al., 2017; Rahmaninezhad et al., 2019; Roodi and Zornberg, 2017; Wang et al., 2016).Simplifying the stress curve with a triangular distribution, a comparison between the in-air residual strain and the pullout residual strain evaluated for the geogrid's monitored portion closer to its head can be made, as for the latter the load acting on this portion is comparable with the one acting on the entire geogrid in the wide-width MS tensile test (that is, the trapezoidal distribution of tensile stresses along the analysed portion is comparable to a rectangular distribution with a value slightly lower than the in-air one). In particular, this comparison highlights that the geogrid's head strains are much higher than those obtained by in-air multi-stage tensile tests, with increments at N = 1 and N = 1000 ranging from 305% to 107% for $A \approx 30\%$ P_R (Figure 7a) and from 258% to 84% for $A \approx 45\%$ P_R (Figure 7b) respectively. Since the load is similar, this result is probably ascribable to the average test rate of pullout MS tests being lower due to the soil confinement. In fact, while in the in-air tests the average test rate of MS phase is almost the same for the all the points of the extensible specimen, in the pullout tests the rate of MS phase decreases from the head to the free rear end due to the soil confinement; therefore, this lower average test rate causes higher residual strains, owing to the HDPE viscous behaviour. In the same graph, the pullout apparent strains evaluated for the entire length of the geogrid are also plotted; at these conditions, under the simplifying hypothesis of a triangular distribution the load acting on the specimen on average is equal to a half of the load applied to the geogrid's head, acting constantly along the specimen. Since both graphs (Figure 7a,b) show that the apparent residual strain values are similar to those obtained by in-air MS tensile tests, it is possible to state that the effects of the reduction in loading application rate during the confined tests (which entail higher strains) compensate for the effects of decrease in loading acting on average (which, by contrast, entail lower strains).

3.3 Effect of cyclic loading history on pullout resistance

The influence of cyclic loading history on the pullout behaviour has also been investigated by comparing the pullout curves for the MS tests and those for the corresponding CRD tests. The comparison is reported in Figure 8a,b for the MS pullout tests at σ'_v = 50 kPa, with loading amplitudes equal to $A \approx 30\%\ P_R$ and $A \approx 45\%\ P_R$ respectively; these tests are qualitatively representative of all those performed. The pullout forces have been obtained subtracting, at the same displacement value, those from tests carried out without the geogrid in order to eliminate the soil-clamp friction. While in the test performed at $A \approx 45\%\ P_R$ and σ'_v = 50 kPa the geogrid has achieved the total horizontal displacement (100 mm) when N = 158 (Figure 8b), ergo the post-cyclic stage being not allowed, in the test at $A \approx 30\%\ P_R$ and σ'_v = 50 kPa the soil-geogrid interface exhibits a cyclically stable behaviour, although it provides pullout resistance values that are lower than those obtained in the CRD test carried out at the same test condition (Figure 8a). Moreover, by observing the MS curve of Figure 8a it is possible to highlight that the soil-geogrid interface still exhibits a very high tangent stiffness when the post-cyclic stage starts, despite its test rate is lower than the one of cyclic stage, where it is considerably higher on average in order to ensure the intended loading amplitude. After that, the soil-geogrid interface stiffness decreases up to the values obtained for the same displacement in the corresponding CRD pullout test. Therefore, the interface exhibited a yielding phase, in agreement with the results of Hirakawa et al. (2003) for geosynthetics tested in-air.

Afterwards, the remaining comparisons for all the vertical effective stresses investigated have been expressed in terms of post-cyclic peak pullout resistance P_R^{PC} (interface's peak pullout resistance obtained in the MS third stage). Figure 9a illustrates P_R^{PC} values obtained in all MS tests with $A \approx 30\%\ P_R$ normalised with respect to P_R, for varying the vertical effective stress. These results suggest that cyclic loading histories induce a reduction in peak pullout resistance that increases with decreasing vertical effective stresses. For these specific test conditions, the post-cyclic peak pullout resistance reaches decreases up to about 28% compared to the values obtained in monotonic pullout tests at the same test conditions. The higher decrease has been measured at the lower investigated σ'_v, while post-cyclic pullout resistance remains almost equal to the corresponding static value at the higher σ'_v.To analyse the effects of cyclic loading on the peak apparent coefficient of friction between soil and geosynthetic, $\mu^P_{s/GSY}$, generally used in the design of reinforced earth structures, the comparison between $\mu^P_{s/GSY}$ evaluated under post-cyclic conditions ($A \approx 30\%\ P_R$) and $\mu^P_{s/GSY}$ obtained by means of CRD pullout tests is plotted in Figure 9b for soil-geogrid interface tested at different vertical effective stresses. The experimental results show that the post-cyclic $\mu^P_{s/GSY}$ decreases with increasing σ'_v, as well as the apparent coefficient of friction under static conditions, due to soil dilatancy at the interface. Moreover, σ'_v being equal, the apparent coefficient of friction between soil and geosynthetic under post-cyclic conditions decreases due to the effects of cyclic loading: the lower the vertical effective stress, the higher the decrease (specifically, the reductions are equal to 28%, 16%, 5% and 2% for σ'_v = 10, 25, 50 and100 kPa respectively). This result is very important as pullout limit state mainly affects the shallow reinforcement levels; therefore, if this decrease is not taken into account, the earth works reinforced with geosynthetics could be wrongly designed.

To better explain the reduction of the interface design parameters in post-cyclic conditions, pullout loading P for varying pullout average strain ε for the i) CRD tests carried out at all the investigated σ'_v (Figure 10a); ii) the MS tests performed at σ'_v = 100 kPa, $A \approx 30$, 45% P_R and the corresponding CRD test (Figure 11a); and iii) the MS tests performed at σ'_v = 50 kPa, $A \approx 30\%$ P_R and the corresponding CRD test (Figure 12a) has been plotted. Before to comment these curves, it is necessary to start by making a clarification: the application of cyclic tensile loading histories on geogrids tested in-air do not induce a material degradation resulting in the reduction of the geosynthetic's tensile strength, according to previous researches (Cardile et al., 2017b; Kongkitkul et al., 2004; Vieira and Lopes, 2013). The main goal of the present research is to comprehend whether or not the behaviour under cyclic pullout conditions (hence in confined conditions) involves a degradation for the soil-geogrid interface resulting in the reduction of the interface parameters (therefore, a reduction of the pullout resistance). For this purpose, the P - ε curves (Figure 10a, Figure 11a, Figure 12a) have been plotted to represent the reinforcement's behaviour under soil confinement condition (for fixed specimen length, test rate and temperature). The soil-geogrid interaction provides P - ε curves that are different for varying the pullout loading conditions (monotonic or cyclic) and the vertical effective stress due to both soil dilatancy at the interface and the reinforcement extensibility (i.e., stiffness). P - ε curves can relate to δ - ε curves (Figure 10b, Figure 11b, Figure 12b) in order to link the displacement of the specimen's first confined section δ to the corresponding pullout average strain value caused by a certain pullout load, for a fixed vertical effective stress. With regard to CRD pullout tests (Figure 10b), when the soil-geogrid interface is in the load transfer phase the δ - ε curve exhibits a pseudo-linear trend (σ'_v = 100 kPa), which tends to curve during the pullout phase (σ'_v = 10, 25, 50 kPa) until reaching a vertical asymptote for pullout failure (constant average strain with increasing δ). δ - ε slope clearly depends only on test rate when the soil-geogrid interface is in the load transfer phase. Once the pullout phase starts, δ - ε slope depends even on σ'_v since the pullout resistances decrease with decreasing σ'_v (Figure 10a).

In pullout multi-stage tests, the first outcome arising from the observation of point 5 versus point 1 in Figure 11b and Figure 12b is that the cyclic loading application caused both a higher geogrid's deformation (due to the geogrid's viscous effects resulting from the application of a loading that can be considered constant on average over time) and a higher head's displacement, with the MS δ - ε slope of the cyclic stage increasing with increasing loading amplitude (pointed out in Figure 11b by means of an arrow-shaped object). This means that the displacements of geogrid's internal points (along the length of the specimen) at the beginning of the MS third phase (point 5) are higher than those mobilised at the same pullout load level P_i (point 1) in the corresponding static test. For a better knowledge, a qualitative trend is plotted in Figure 11c and Figure 12c (square c-1): by comparing them, the lower the vertical effective stress, the higher the displacements. These representations allow understanding how these higher displacements obtained under cyclic loading move the interface towards a configuration closer to pullout failure than the corresponding static test.

By analysing the third stage, Figure 11b and Figure 12b show that the MS δ-ε curve at the beginning of this phase restarts with a trend similar to the one of CRD δ-ε curve at the same strain level $\varepsilon_{0-2} = \varepsilon_{0-5}$ (point 5 versus point 2): trends get back similar as both are now displacement-controlled pullout tests at the same test rate. Specifically, it looks like the CRD δ-ε curve shifts down (path 5-7) of an amount δ_{2-5} equal to the difference between the cyclic (δ_{1-5}) and the static (δ_{1-2}) displacements of the specimen's first confined section reached at the same pullout average strain level (Figure 12b).

Moreover, during the third stage the interface tries again to mobilise the same pullout strength that it would have mobilised if the cyclic stage hadn't occurred (reinforcement has no degradation per se), showing a hardening curve (incremental pullout stiffness in the path 5-6b is higher than the one in path 2-4, Figure11a and Figure 12a). However, this could be not possible since the cyclic loading contributed to use up more quickly the geogrid's portion on which the mobilisation of the interaction mechanisms withstands the applied load; that is, these cyclic loading effects (pointed out in Figure 11b and Figure 12b by means of an arrow-shaped object) could lead the interface a little bit closer to the pullout failure , compared to an entirely monotonic loading. In fact, if the development of the interaction mechanisms along the geogrid hadn't gone further, the MS δ- ε curve would have followed the "ideal" trend (dash-dot line in path 5-7, Figure 12b), i.e. the difference between MS and CRD displacements of the specimen's first confined section reached at the same pullout average strain level would have continued to be always δ_{2-5} (caused by the cyclic load application). Instead, the actual MS δ- ε curve deviates from the "ideal" path 5-7 due to the cyclic loading effects, which cause the interface degradation; this means that the geogrid starts to deform fewer when a certain head's displacement is reached, mobilising a lower pullout strength.

These cyclic loading effects can be appreciate better by considering the displacements qualitative distribution of the geogrid's internal points when δ = 100 mm has been reached: Figure 11c and Figure 12c, square c-2 show that the displacements of the geogrid's internal points representing 6b are higher than those representing 6a, and this result is because the cyclic loading pushed towards the pullout process; in other words, the geogrid starts to deform fewer approaching the pullout limit state earlier. Clearly, the smaller the displacements of the geogrid's internal points, the more ideal the δ - ε trend.

Summarising, to reach the pullout average strain corresponding to the peak pullout resistance P_R obtained under static conditions is theoretically always possible, unless pullout failure occurs first (vertical asymptote). This assertion can be explained by considering a fictitious extension of the MS δ - ε curve (dashed lines, Figure 11b and Figure 12b): the soil-geogrid interface has to make a further head's displacement in order to achieve P_R (i.e. the interface can mobilise P_R with a head's displacement greater than the one under static condition). For instance, the interface tested at σ'_v = 100 kPa would mobilise P_R with both the investigated amplitudes in case it could carry out the further increment plotted in Figure 11b ($\delta_{6b\text{-}8}$ for $A \approx 30\%$ P_R and $\delta_{6'b\text{-}8'}$ for $A \approx 45\%$ P_R respectively). This result affects the peak apparent coefficient of friction between soil and geosynthetic; in fact, $\mu^{P}_{s/GSY}$ (Figure 9b) evaluated under post-cyclic conditions ($A \approx 30\%$ P_R) is almost equal to the one obtained in the corresponding static pullout test for σ'_v = 100 kPa (only a very slight degradation of the interface occurred). In case the limitation due to the clamp maximum displacement allowed by the laboratory apparatus does not exist, the soil-geogrid interface analysed in this research can mobilise P_R at σ'_v = 100 kPa even under post-cyclic loading with amplitudes up to $A \approx 45\%$ P_R.

Instead, for the interface at σ'_v = 50 kPa to reach the pullout average strain corresponding to P_R is more difficult as the head's displacement to be done is much higher (this increasing with decreasing vertical effective stress): the MS δ - ε trend is curved (as well as the CRD one) as the pullout phase has been reached (Figure 12b) and the displacements of the geogrid's internal points (6b trend in Figure 12c, square c-2) are pushing further towards the achievement of pullout failure (that is, the cyclic loading degraded the interface). This means that the pullout loading cannot increase further and, consequently, $\mu^{P}_{s/GSY}$ evaluated under post-cyclic conditions is lower than $\mu^{P}_{s/GSY}$ obtained in the corresponding CRD pullout test.

3.4 Nodal displacements

Finally, in order to explain the different behaviour of the soil-reinforcement interface when the cyclic loading generates a load transfer mechanism or the pullout failure, the actual distributions of the transversal rib displacements along the geogrid for different numbers of cycles have been plotted in Figure 13a,b, for $A \approx 30\%\ P_R$ and σ'_v = 10 and 100 kPa respectively. In Figure 13a, for vertical effective stress equal to 10 kPa, it is possible to observe that the reinforcement almost reached the pullout limit state during the cyclic stage (two adjacent curves are parallel to each other), with the third stage still being allowed (as the reached head's displacement is lower than 100 mm). This means that the cyclic loading entailed a significant reduction of the pullout resistance during the CRD third stage, caused by higher displacements along the geogrid that pushed towards the pullout failure. Since the mobilised soil shear-strength angle depends on soil-geogrid relative sliding, the interaction mechanisms along the interface's points (Bergado et al., 1993; Calvarano et al., 2014; Cardile et al., 2017a; Dyer, 1985; Jacobs et al., 2014; Moraci et al., 2017; Palmeira, 2009; Sieira et al., 2009; Zhou et al., 2012; Ziegler and Timmers, 2004) mobilised pullout strengths lower than those mobilised under static conditions. These values are as close as possible to the lowest that can be reached under static conditions, i.e. they are characteristic of the residual phase in the pullout static curve at σ'_v = 10 kPa (strain-softening pullout behaviour at lower σ'_v as shown in Moraci and Recalcati, 2006). On the other hand, for σ'_v = 100 kPa, the reinforcement is still in the load transfer phase when the cyclic stage is over: the interaction mechanisms developed a pullout mechanism along the active length that is markedly progressive (Figure 13b). In this case, a “supply” of resistance is still available in the post-cyclic stage for all the above reasons. The interaction mechanisms mobilised strength values almost equal to $P_{R,}$ which happens to coincide with the ultimate resistance that can be reached, as the CRD curve at σ'_v = 100 kPa exhibits a strain-hardening pullout behaviour (typical of higher vertical effective stresses as shown in Moraci and Recalcati, 2006).

4 CONCLUSIONS

The paper deals with the results of several pullout tests carried out on an HDPE geogrid-granular soil interface subjected to multi-stage loading conditions and different vertical effective stresses (σ'_v = 10, 25, 50, 100 kPa). Cyclic and post-cyclic conditions were investigated by means of a multistage procedure, applying different cyclic loading histories characterised by a high frequency (f=1 Hz).

To define when the behaviour of soil-reinforcement interface is stable/unstable from a point of view linked to the cyclic loadings application, a criterion has been established.

The results have showed that the soil-geogrid interface behaviour is dependent on both the cyclic loading amplitude and vertical effective stress. The stability of soil-geogrid interface during the cyclic phase starts getting worse with increasing cyclic loading amplitude, entailing the possible achievement of the pullout limit state, while the increasing of the vertical effective stress σ'_v plays a stabilising role.

The analysis of the cumulative strain mobilised in the specimen at the end of each corresponding cycle highlighted that it increases with increasing cyclic loading amplitude and numbers of cycles and, *N* being equal, increases with increasing vertical effective stress. By comparing the results of residual strain evaluated for the geogrid's monitored portion closer to its head with those obtained by wide-width tensile multi-stage tests, the pullout cyclic residual strain happens to be higher since the average test rate of pullout MS tests is lower due to the soil confinement.

With regard to pullout resistances, the results have showed that cyclic loading histories can involve a reduction of the interface parameters considering a certain combination of vertical effective stress and cyclic loading amplitude *A*, for the investigated frequency: the lower the vertical effective stress, the higher the reduction, *A* being equal. For the specific test conditions, the post-cyclic peak pullout resistance reaches decreases up to 28% at the lower σ'_v investigated, while it remains almost equal to the corresponding monotonic value at the higher σ'_v.

The decreasing of the interface parameters can be explained by the progressive pullout mechanism of the soil-geogrid interface: the load is transferred on a geogrid's portion that increases quickly during the cyclic phase, involving a reduction of the "supply" of pullout resistance during the post-cyclic phase that increases with decreasing vertical effective stress and with increasing cyclic loading amplitude. To reach the static peak pullout resistance P_R is theoretically always possible even under cyclic conditions, unless pullout failure occurs: the interface can mobilise P_R with a head's displacement greater than the one under static condition.

The preferred option to design GRS structures in the best way possible would be to use peak apparent coefficients of friction between soil and geosynthetic, $\mu^{P}_{s/GSY}$, varying with the depth where the reinforcement is embedded. If it be so, since pullout limit state mainly affects the shallow reinforcement levels, the $\mu^{P}_{s/GSY}$ reduction arising under possible cyclic loading has to be taken into account. Specifically, the lower the vertical effective stress, the higher the reduction.

List of notation

A	Cyclic tensile loading amplitude (kN/m)
CRD	Constant rate of displacement (mm/min)
CSR	Constant strain rate (%/min)
D_{50}	Average grain size (mm)
f	Frequency of cyclic load (Hz)
GRS	Geosynthetic-reinforced soil (-)
$HDPE$	High-density polyethylene (-)
$J_{\mathrm{sec}\,2\%}$	Secant tensile stiffness at 2% strain (0.2%/min strain rate) (kN/m)
$J_{\mathrm{sec}\,2\%\,(\mathrm{ISO})}$	Secant tensile stiffness at 2% strain (20%/min strain rate, STANDARD ISO 10319) (kN/m)
L_R	Length of geogrid (m)
MS	Multi-stage (-)
N	Number of cycles (-)
P	Pullout load per unit width (kN/m)
P_i	Pullout load (per unit width) representative of serviceability conditions (kN/m)
P_R	Peak pullout resistance (per unit width) obtained by pullout tests under static conditions (kN/m)
P_R^{PC}	Peak pullout resistance (per unit width) obtained by pullout tests under multi-stage conditions (kN/m)
RH	Relative humidity (%)
$T_{\max}$	Maximum tensile strength per unit width (monotonic test at 0.2%/min strain rate) (kN/m)
$T_{\max\,(\mathrm{ISO})}$	Maximum tensile strength per unit width (monotonic test at 20%/min strain rate, STANDARD ISO 10319) (kN/m)
U	Uniformity coefficient (-)
w_{opt}	Optimum water content (%)
γ_d	Dry unit weight (kN/m^3)
$\gamma_{d\,\max}$	Maximum dry unit weight (kN/m^3)
δ	Displacement of the first confined section of specimen (mm)
$\Delta\delta_i^e$	Cumulative cyclic displacement of the specimen's rear end (mm)
$\Delta\delta_i^h$	Cumulative cyclic displacement of the specimen's first confined section (mm)
$\Delta\delta_{part,i}^e$	Cyclic displacement's increment of the specimen's rear end reached during each cyclic loading (mm)
$\Delta\delta_{part,i}^h$	Cyclic displacement's increment of the specimen's head reached during each cyclic loading (mm)

ε	Pullout average strain (%)
$\varepsilon_{\max}$	Tensile strain for $T_{\max}$ (monotonic test at 0.2%/min strain rate) (%)
$\varepsilon_{\max\,(\mathrm{ISO})}$	Tensile strain for $T_{\max\,(\mathrm{ISO})}$ (monotonic test at 20%/min strain rate, STANDARD ISO 10319) (%)
ε_r	Residual strains caused by cyclic loading when the cyclic loading returns to Pi (%)
ε'	Strain rate (%/min)
$\mu_{S/GSY}^{P}$	Peak apparent coefficients of friction between soil and geosynthetic (-)
$\sigma_v^{'}$	Vertical effective stress (kN/m^2)
$\phi_p^{'}$	Soil peak shear-strength angle (°)
$\phi_{cv}^{'}$	Soil shear-strength angle at constant volume (°)

Tables

Table 1 Wide-width tensile test results of the geogrid used in this research.

$T_{\max\,(ISO)}$ [kN/m] ($\varepsilon' = 20\,\%$ per minute)	$T_{\max}$ [kN/m] ($\varepsilon' = 0.2\,\%$ per minute)	$\varepsilon_{\max\,(ISO)}$ [kN/m] ($\varepsilon' = 20\,\%$ per minute)	$\varepsilon_{\max}$ [kN/m] ($\varepsilon' = 0.2\,\%$ per minute)	$J_{\sec\,2\,\%\,(\mathrm{ISO})}$ [kN/m] ($\varepsilon' = 20\,\%$ per minute)	$J_{\sec\,2\,\%}$ [kN/m] ($\varepsilon' = 0.2\,\%$ per minute)
159	103.5	12.2	14.5	2454	1525

Table 2 MS pullout testing plan.

Test	N (planned)	N (actually-made)	σ_v' [kPa]	P_i [kN/m]	A [kN/m]
01	1000	1000	10	≈35%P_R (10 kPa)	≈30%P_R (10 kPa)
02	1000	20	10	≈35%P_R (10 kPa)	≈45%P_R (10 kPa)
03	1000	1000	25	≈35%P_R (25 kPa)	≈30%P_R (25 kPa)
04	1000	148	25	≈35%P_R (25 kPa)	≈45%P_R (25 kPa)
05	1000	1000	50	≈35%P_R (50 kPa)	≈30%P_R (50 kPa)
06	1000	158	50	≈35%P_R (50 kPa)	≈45%P_R (50 kPa)
07	1000	1000	100	≈35%P_R (100 kPa)	≈30%P_R (100 kPa)
08	1000	1000	100	≈35%P_R (100 kPa)	≈45%P_R (100 kPa)

FIGURES

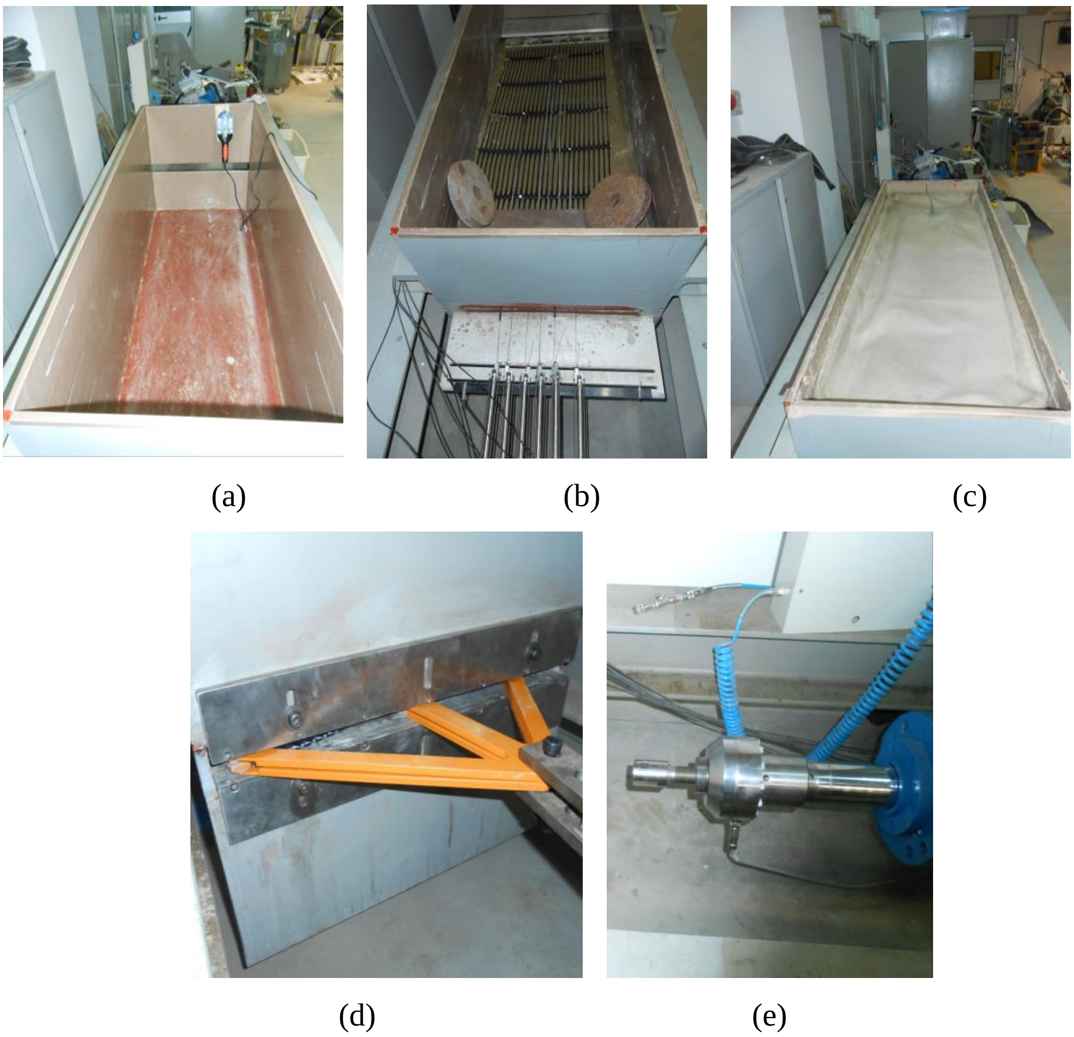

Figure 1. Apparatus used for pullout testing: pullout steel box (a); soil-geogrid specimen and LVDT (b); air bag (c); clamp and sleeves (d), hydraulic actuator and load cell (e).

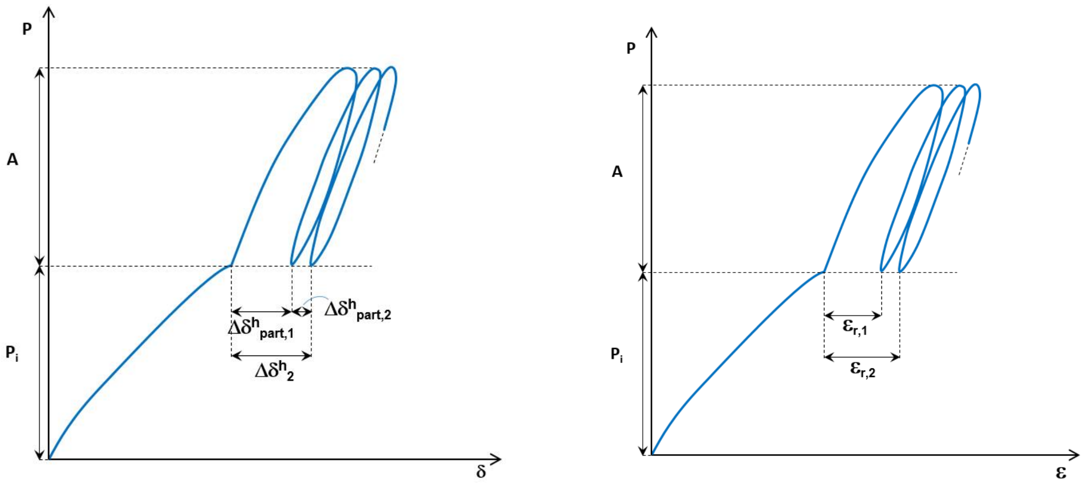

(a) (b)

Figure 2. Schematic representation of different parameters obtained during hysteresis loops in multi-stage tests: P-δ plane (a); P-ε plane (b).

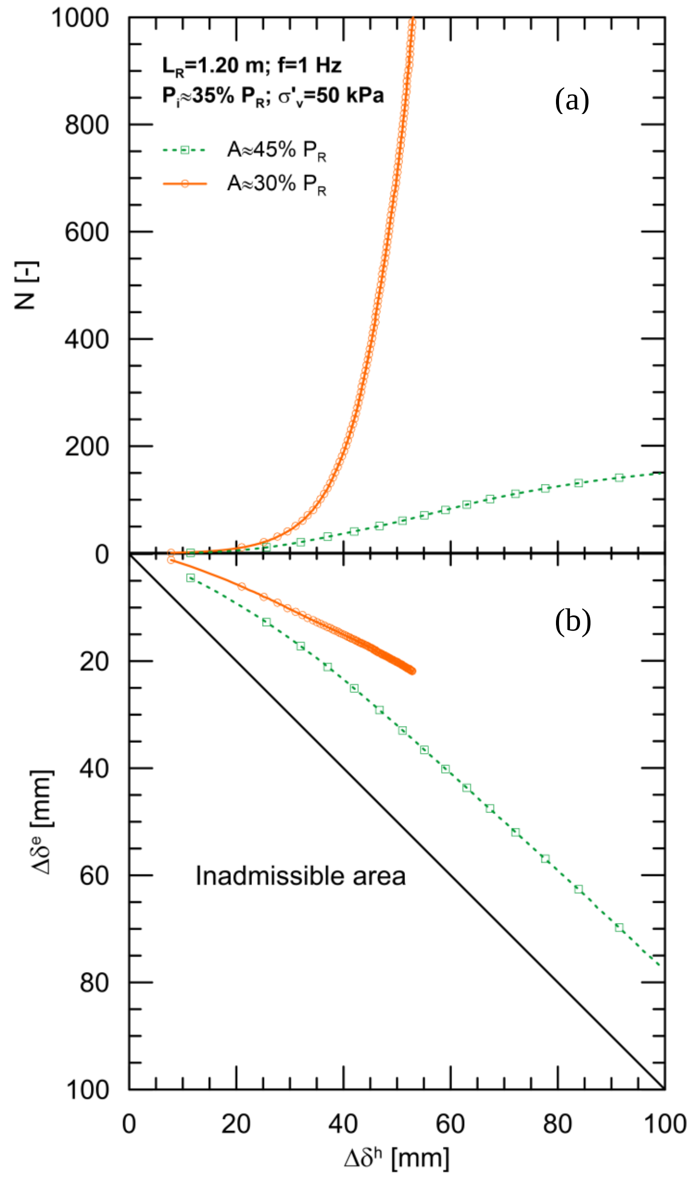

Figure 3. Number of loading cycles versus cumulative cyclic displacement measured at the first confined section of specimen (a), and $\Delta\delta^h$ *versus cumulative cyclic displacement measured at the rear end of the specimen (b) for* $A \approx 30\%\ P_R$, $45\%\ P_R$ *and* $\sigma'_v = 50$ *kPa.*

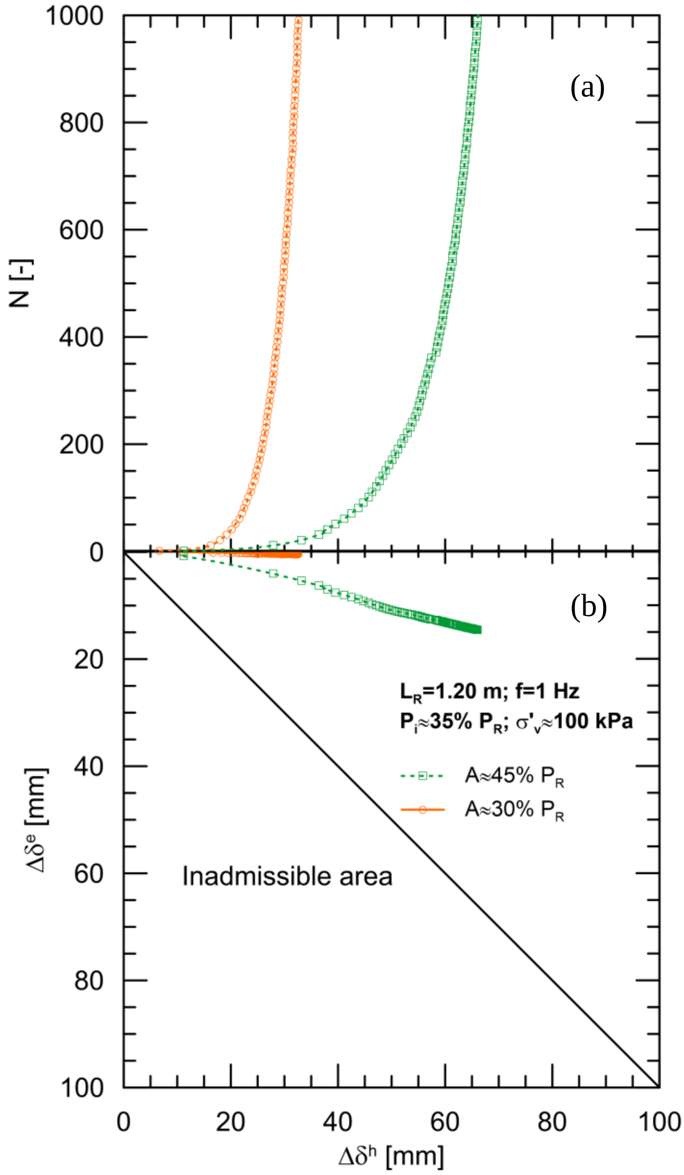

Figure 4. Number of loading cycles versus cumulative cyclic displacement measured at the first confined section of specimen (a), and $\Delta\delta^h$ versus cumulative cyclic displacement measured at the rear end of the specimen (b) for $A \approx 30\%\ P_R$, $45\%\ P_R$ and $\sigma'_v = 100$ kPa.

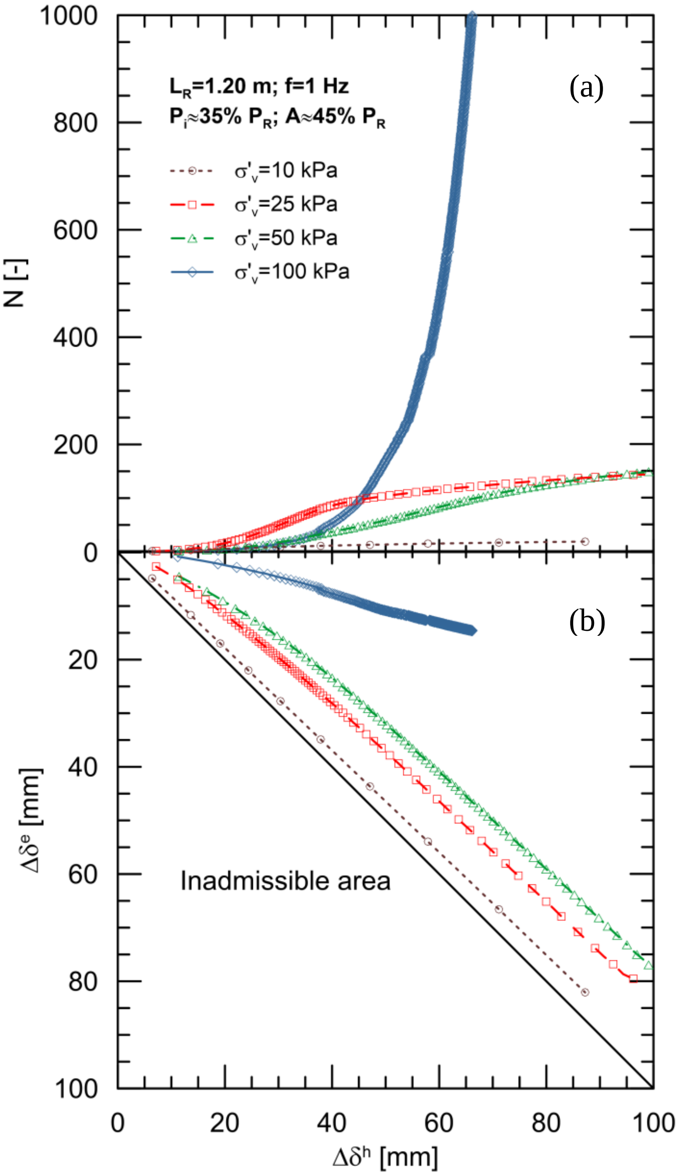

Figure 5. Number of loading cycles versus cumulative cyclic displacement of the specimen's first confined section (a) and $\Delta\delta^h$ *versus cumulative cyclic displacement of the specimen's rear end (b) for varying* σ'_v *at* $A \approx 45\%\ P_R$.

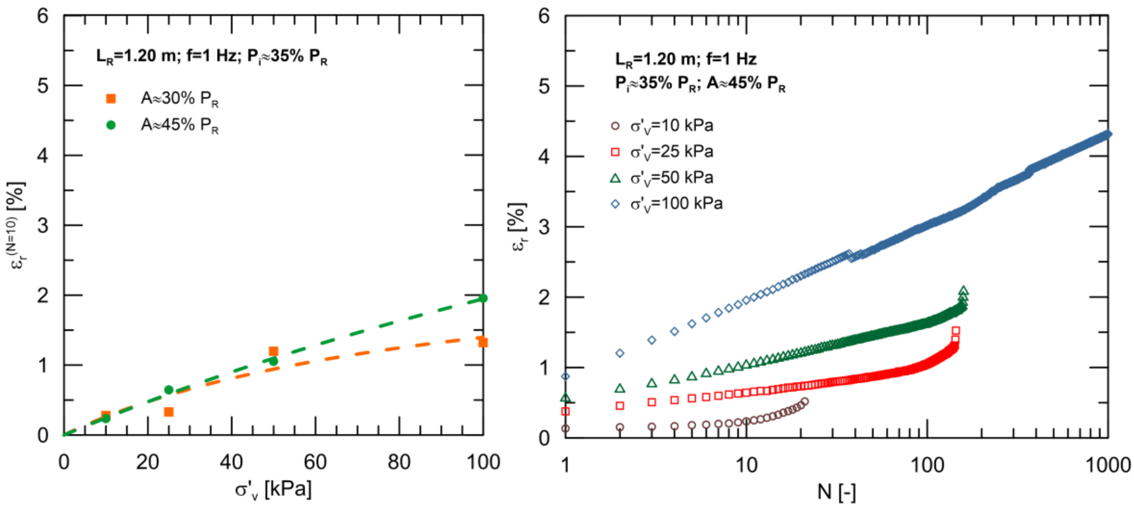

(a) (b)

Figure 6. Residual strain at loading cycle N = 10 versus vertical effective stress, for $A \approx 30\%\ P_R$ and $45\%\ P_R$ (a); and residual strain for varying number of loading cycles at different vertical effective stresses and $A \approx 45\%\ P_R$ (b).

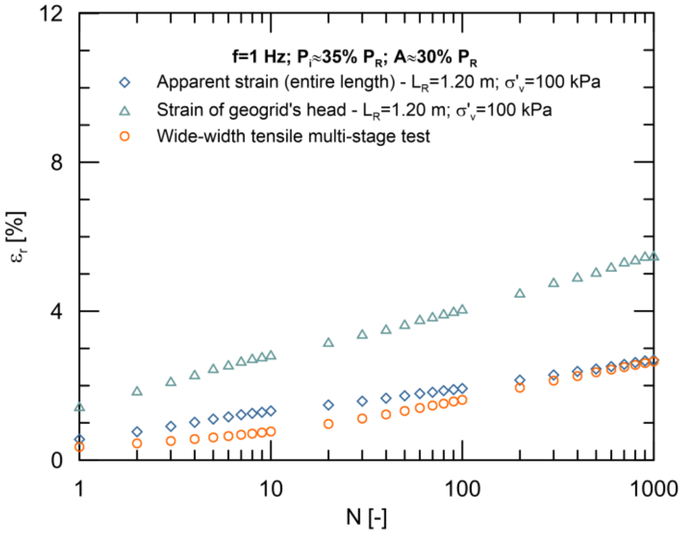

(a)

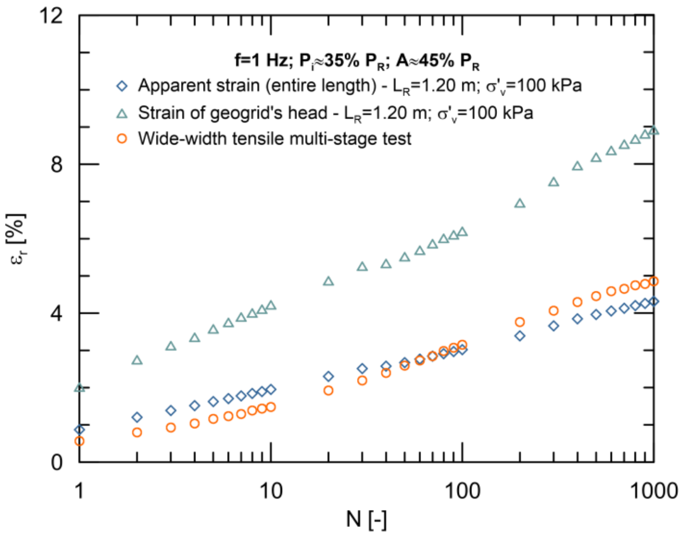

(b)

Figure 7. Residual strain evaluated for the entire length of the geogrid and its monitored portion closer to the head, for varying number of loading cycles at σ_v' *= 100 kPa, A ≈ 30%* P_R *(a) and* σ_v' *= 100 kPa, A ≈ 45%* P_R *(b), and comparison with the corresponding wide-width tensile tests.*

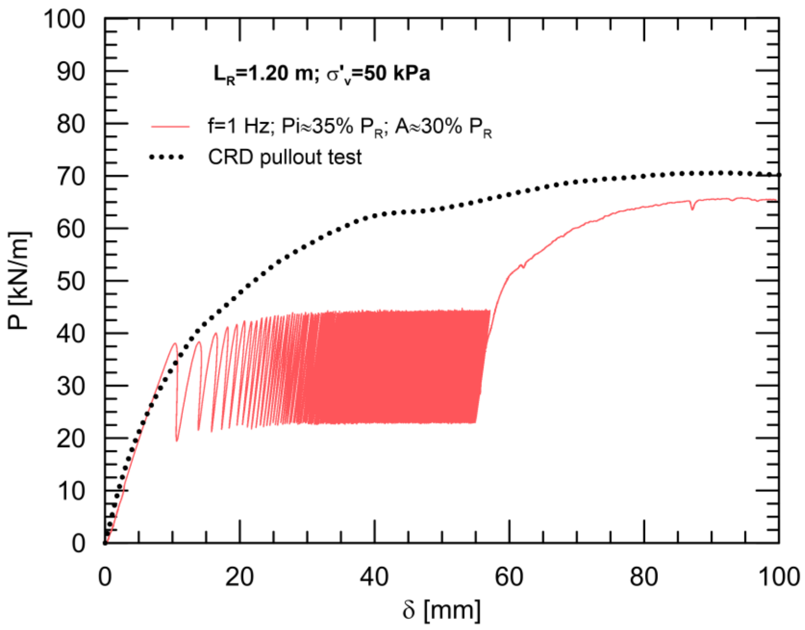

(a)

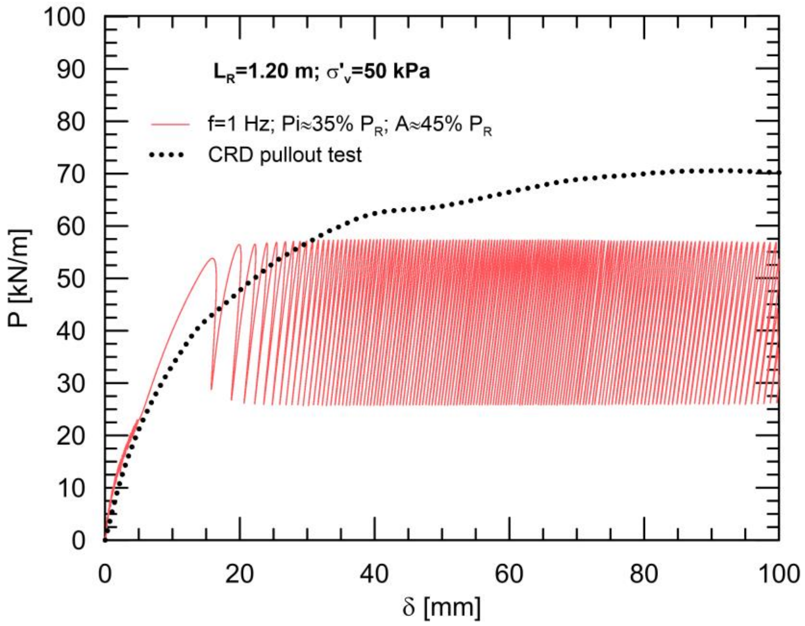

(b)

Figure 8. Comparison between load-displacement trends obtained in CRD and multistage conditions for tests with σ'_v *=50 kPa, at* $A \approx 30\%\ P_R$ *(a) and* $A \approx 45\%\ P_R$ *(b) respectively.*

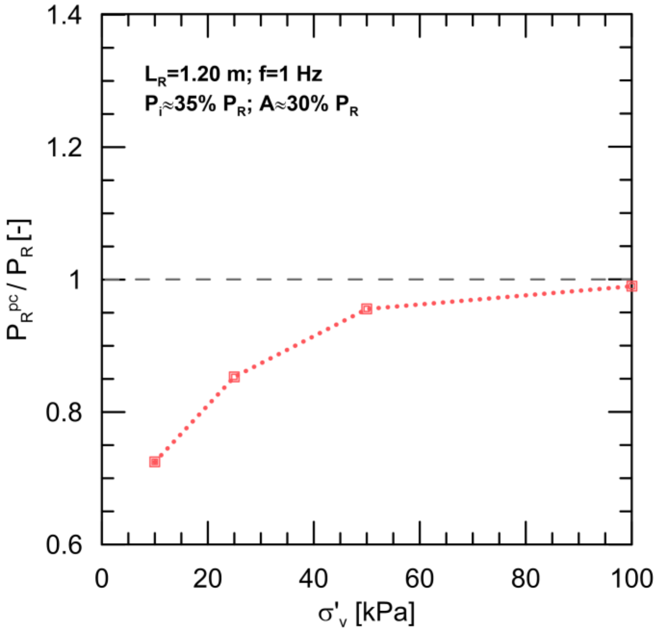

(a)

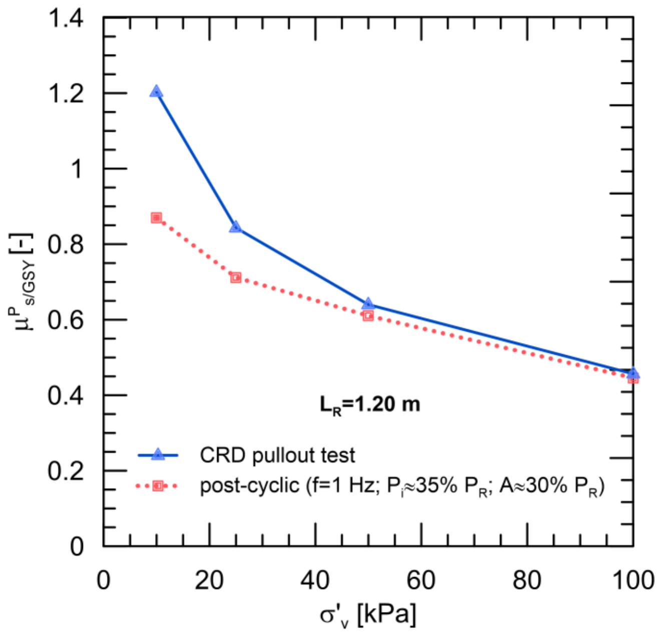

(b)

Figure 9. Normalised post-cyclic peak pullout resistance (a) and peak apparent coefficient of friction (b) for varying vertical effective stress, considering CRD and multi-stage tests at A ≈ 30% P_R.

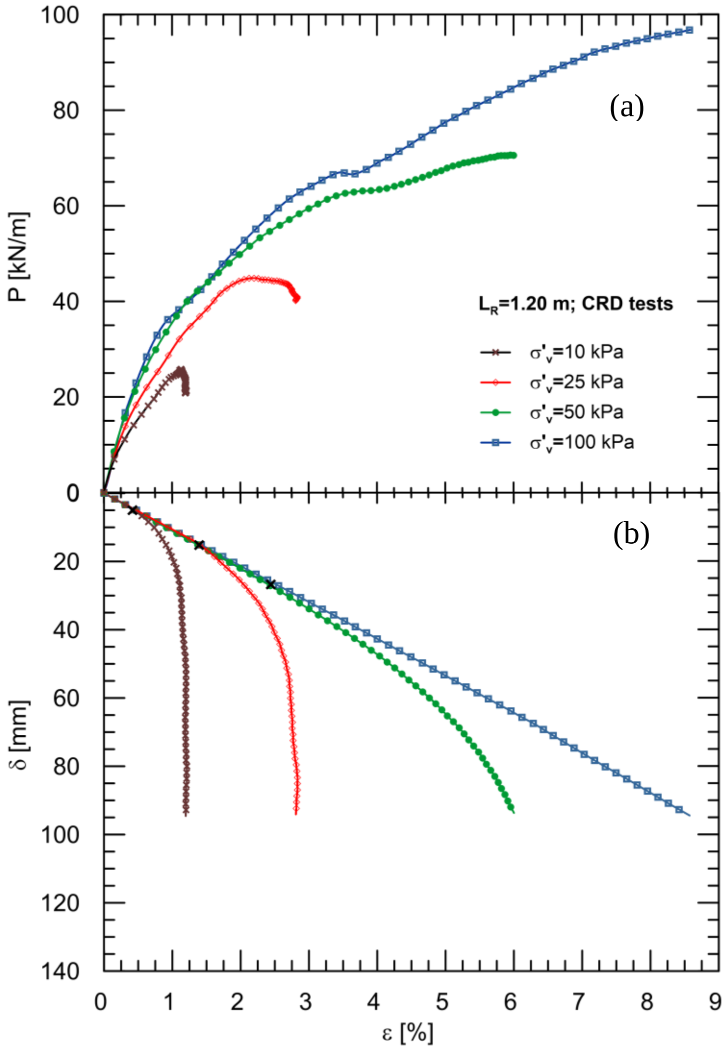

Figure 10. P- ε (a) and δ-ε (b) trends obtained in CRD conditions for different vertical effective stresses.

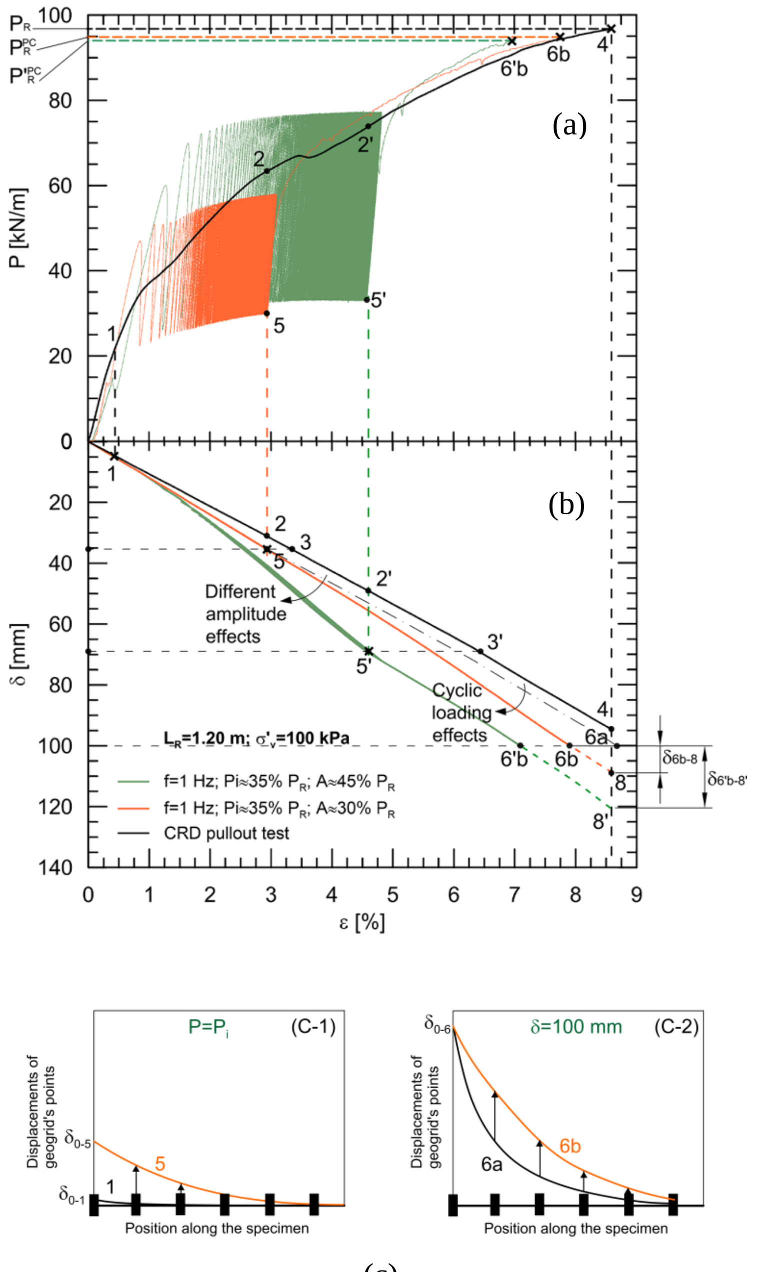

Figure 11. Comparison between P- ε (a) and δ-ε (b) trends obtained in CRD and multistage conditions for tests with σ'_v = 100 kPa, at A ≈ 30-45% P_R, and qualitative distribution of the geogrid's points displacements at the same pullout load level P_i for CRD test and MS test at N=1000 (c-1) and at δ = 100 mm for MS test following the "ideal" or the real path (c-2).

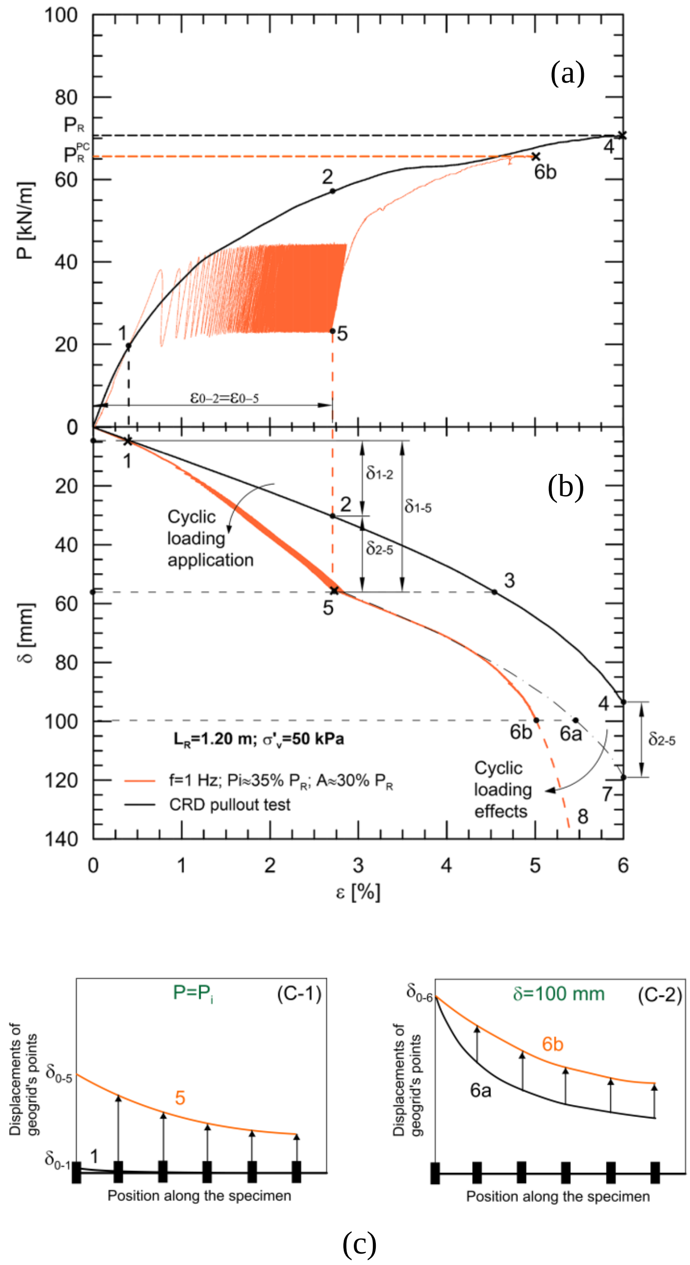

Figure 12. Comparison between P- ε (a) and δ-ε (b) trends obtained in CRD and multistage conditions for tests with σ_v' =50 kPa, at A ≈ 30% P_R, and qualitative distribution of the geogrid's points displacements at the same pullout load level P_i for CRD test and MS test at N=1000 (c-1) and at δ = 100 mm for MS test following the "ideal" or the real path (c-2).

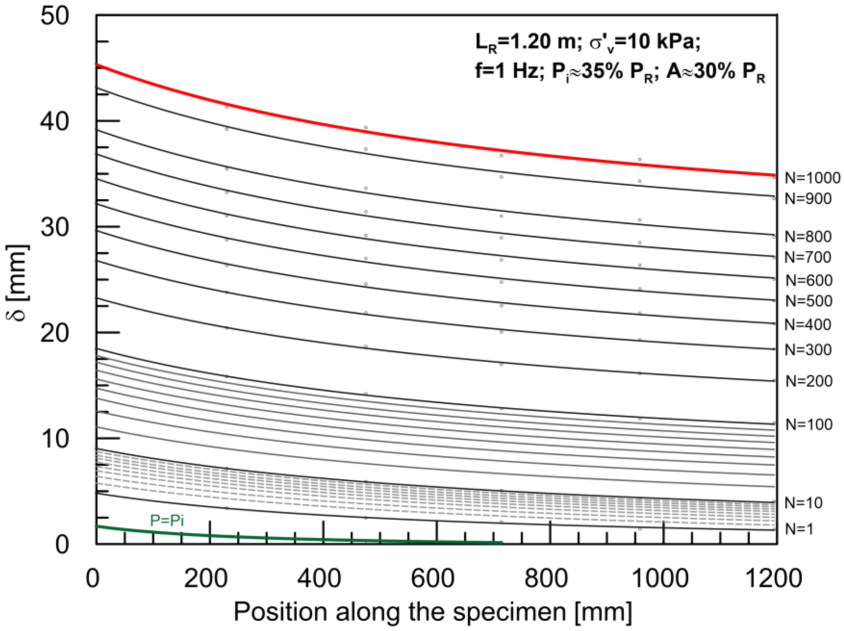

(a)

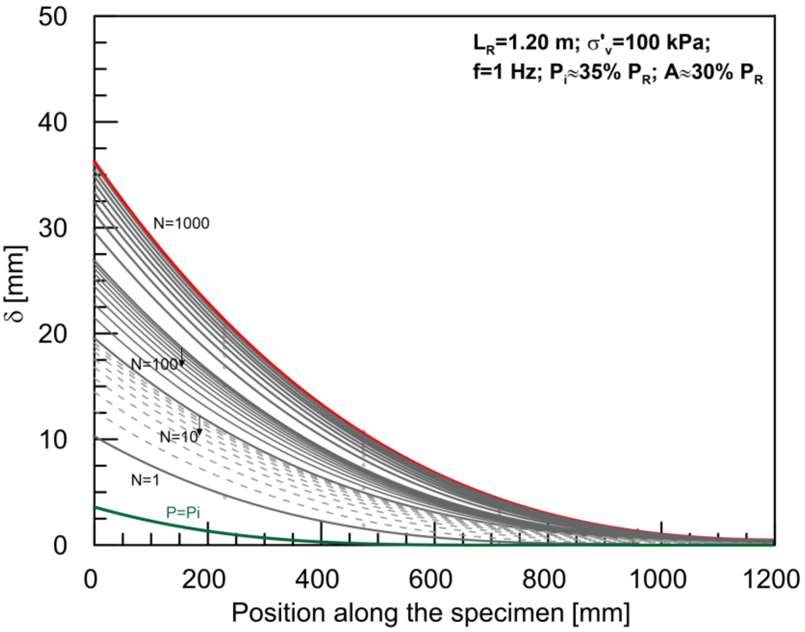

(b)

Figure 13. Distributions of the nodal displacements along the reinforcement for different numbers of cycles, for specimens tested at $A \approx 30\%\ P_R$ and $\sigma'_v = 10$ kPa (a); $A \approx 30\%\ P_R$ and $\sigma'_v = 100$ kPa (b) respectively.

5 REFERENCES

AASHTO T 99, 2015. Standard Method of Test for Moisture-Density Relations of Soils Using a 2.5-kg (5.5-lb) Rammer and a 305-mm (12-in.) Drop, American Association of State Highway and Transportation Officials (AASHTO), Washington, DC, USA.

ASTM D2487-17, 2017. Standard Practice for Classification of Soils for Engineering Purposes (Unified Soil Classification System), ASTM International, West Conshohocken, PA.

Abramento, M., 1995. Analysis of pullout tests for planar reinforcements in soil. Journal of Geotechnical Engineering 121 (6), 476-485.

Alonso-Marroquín, F., Herrmann, H.J., 2004. Ratcheting of Granular Materials. Physical Review Letters 92 (5), 543011-543014.

ASTM D1557-12e1, 2012. Standard Test Methods for Laboratory Compaction Characteristics of Soil Using Modified Effort (56,000 ft-lbf/ft3 (2,700 kN-m/m3)), ASTM, West Conshohocken, PA, USA

ASTM D698-12e2, 2012. Standard Test Methods for Laboratory Compaction Characteristics of Soil Using Standard Effort (12 400 ft-lbf/ft3 (600 kN-m/m3)), ASTM, West Conshohocken, PA, USA

Ausilio, E., Conte, E., Dente, G., 2000. Seismic stability analysis of reinforced slopes. Soil dynamics and earthquake engineering 19, 159-172.

Bathurst, R.J., Allen, T., Walters, D., 2004. Reinforcement loads in geosynthetic walls and the case for a new working stress design method, Mercer Lecture. 3rd European Geosynthetics Conference Eurogeo 3, Monaco, Germany, pp. 19-32.

Bathurst, R.J., Cai, Z., 1995. Pseudo-static seismic analysis of geosynthetic-reinforced segmental retaining walls. Geosynthetics International 2 (5), 787-830.

Bathurst, R.J., Ezzein, F.M., 2017. Insights into geogrid–soil interaction using a transparent granular soil. Géotechnique Letters 7, 179-183.

Bergado, D.T., Shivashankar, R., Alfaro, M.C., Chai, J.-C., Balasubramaniam, A.S., 1993. Interaction behaviour of steel grid reinforcements in a clayey sand. Geotechnique 43 (4), 589-603.

Biondi, G., Cascone, E., Maugeri, M., 2014. Displacement versus pseudo-static evaluation of the seismic performance of sliding retaining walls. Bulletin of Earthquake Engineering, 12(3), 1239-1267.

Cai, Z., Bathurst, R.J., 1996a. Deterministic sliding block methods for estimating seismic displacements of earth structures. Soils Dynamics and Earthquake Engineering 15, 255-268.

Cai, Z., Bathurst, R.J., 1996b. Seismic-induced permanent displacement of geosynthetic-reinforced segmental retaining walls. Canadian Geotechnical Journal 33, 937-955.

Calvarano, L.S., Gioffrè, D., Cardile, G., Moraci, N., 2014. A stress transfer model to predict the pullout resistance of extruded geogrids embedded in compacted granular soils, 10th International Conference on Geosynthetics, ICG 2014, Berlin, Germany.

Calvetti, F., di Prisco, C., 2010. Discrete numerical investigation of the ratcheting phenomenon in granular materials. Comptes Rendus Mécanique 338 (10-11), 604-614.

Capilleri, P.P., Ferraiolo, F., Motta, E., Scotto, M., Todaro, M., 2019. Static and dynamic analysis of two mechanically stabilized earth walls. Geosynthetics International.

Carbone, L., Gourc, J.P., Carrubba, P., Pavanello, P., Moraci, N., 2015. Dry friction behaviour of a geosynthetic interface using inclined plane and shaking table tests. Geotextiles and Geomembranes 43 (4), 293-306.

Cardile, G., Calvarano, L.S., Gioffrè, D., Moraci, N., 2014. Experimental evaluation of the pullout active length of different geogrids, 10th International Conference on Geosynthetics, ICG 2014, Berlin, Germany.

Cardile, G., Gioffrè, D., Moraci, N., Calvarano, L.S., 2017a. Modelling interference between the geogrid bearing members under pullout loading conditions. Geotextiles and Geomembranes 45 (3), 169-177.

Cardile, G., Moraci, N., Calvarano, L.S., 2016a. Geogrid pullout behaviour according to the experimental evaluation of the active length. Geosynthetics International 23 (2), 194-205.

Cardile, G., Moraci, N., Pisano, M., 2016b. In-air Tensile Load-strain Behaviour of HDPE Geogrids Under Cyclic Loading. Procedia Engineering 158, 266-271.

Cardile, G., Moraci, N., Pisano, M., 2017b. Tensile behaviour of an HDPE geogrid under cyclic loading: experimental results and empirical modelling. Geosynthetics International 24 (1), 95-112.

Carrubba, P., Colonna, P., 2000. A comparison of numerical methods for multi-tied walls. Computers and Geotechnics 27 (2), 117-140.

Carrubba, P., Montanelli, F., Moraci, N., 2000. Long-term behaviour of an instrumented wall reinforced with geogrids, 2nd European Conference on Geosynthetics, Bologna, Italy.

Di Filippo G., Biondi G., Moraci N., 2019. Seismic performance of geosynthetic-reinforced retaining walls: experimental tests VS numerical predictions. 7th lnternational Conference on Earthquake Ge-otechnical Engineering.

Dyer, M.R., 1985. Observations of the stress distribution in crushed glass with applications to soil reinforcement, Magdalene College. University of Oxford, Michaelmas Term, Ph.D. Thesis, p. 220.

El-Emam, M.M., Bathurst, R.J., 2004. Experimental design, instrumentation and interpretation of reinforced soil wall response using a shaking table. Intemational Joumal of Physical Modelling in Geotechnics 4, 13-32.

El-Emam, M.M., Bathurst, R.J., 2005. Facing contribution to seismic response of reduced-scale reinforced soil walls. Geosynthetics International 12 (6), 344-344.

Franca, F.A.N., Bueno, B.S., 2011. Creep behavior of geosynthetics using confined accelerated tests. Geosynthetics International 18 (5), 242-254.

Gaudio, D., Masini, L., Rampello, S., 2018. A performance-based approach to design reinforced-earth retaining walls. Geotextiles and Geomembranes 46 (4), 470-485.

Hatami, K., Bathurst, R.J., 2000. Effect of structural design on fundamental frequency of reinforced-soil retaining walls. Soil dynamics and earthquake engineering 19, 137-157.

Hirakawa, D., Kongkitkul, W., Tatsuoka, F., Uchimura, T., 2003. Time-dependent stress–strain behaviour due to viscous properties of geogrid reinforcement. Geosynthetics International 10 (6), 176-199.

Huang, C.-C., Chou, L.H., Tatsuoka, F., 2003. Seismic displacements of geosynthetic-reinforced soil modular block walls. Geosynthetics International 10 (1), 2-23.

ISO 10319:2015. GeosyntheticsWide-width Tensile Test. International Organization for Standardization, Geneva, Switzerland.

Izawa, J., Kuwano, J., Ishihara, Y., 2004. Centrifuge tilting and shaking table tests on the RSW with different soils, 3rd Asian Regional Conference on Geosynthetics, Seoul, Korea, pp. 803-810.

Jacobs, F., Ziegled, M., Vollmert, L., Ehrenberg, H., 2014. Explicit design of geogrids with a nonlinear interface model, X International conference on Geosynthetics, Berlin, Germany.

Jewell, R.A., 1990. Reinforcement bond capacity. Geotechnique 40 (3), 513-518.

Kongkitkul, W., Hirakawa, D., Tatsuoka, F., Uchimura, T., 2004. Viscous deformation of geosynthetic reinforcement under cyclic loading conditions and its model simulation. Geosynthetics International 11, 73-99.

Kongkitkul, W., Tatsuoka, F., Hirakawa, D., 2007a. Effects of reinforcement type and loading history on the deformation of reinforced sand in plane strain compression. Soils and foundations 47 (2), 395-414.

Kongkitkul, W., Tatsuoka, F., Hirakawa, D., 2007b. Rate-dependent load-strain behaviour of geogrid arranged in sand under plane strain compression. Soils and foundations 47 (3), 473-491.

Koseki, J., Bathurst, R.J., Guler, E., Kuwano, J., Maugeri, M., 2006. Seismic stability of reinforced soil walls, 8th International Conference on Geosynthetics, Yokohama. Japan.

Koseki, J., Nakajima, S., Tateyama, M., Watanabe, K., Shinoda, M., 2009. Seismic performance of geosynthetic-reinforced soil retaining walls and their performance-base design in Japan, Performance-Based Design in Earthquake Geotechnical Engineering, Tokyo, Japan.

Lee, K.Z.Z., Chang, N.Y., Ko, H.Y., 2010. Numerical simulation of geosynthetic-reinforced soil walls under seismic shaking Geotextiles and Geomembranes 28 (4), 317-334.

Leshchinsky, D., 2009. On Global Equilibrium in Design of Geosynthetic Reinforced Walls. Journal of Geotechnical and Geoenvironmental Engineering 135 (3), 309-315.

Leshchinsky, D., Ling, H., Hanks, G., 1995. Unified design approach to geosynthetics reinforced slopes and segmental walls. Geosynthetics International 2 (5), 845-881.

Leshchinsky, D., Kang, B., Han, J., Ling, H., 2014. Framework for Limit State Design of Geosynthetic-Reinforced Walls and Slopes. Transportation Infrastructure Geotechnology 1, 129-164.

Ling, H., Leshchinsky, D., 2005. Failure Analysis of Modular-Block Reinforced-Soil Walls during Earthquakes. Journal of Performance of Constructed Facilities 19 (2), 117-123.

Ling, H.I., Leshchinsky, D., Chou, N.N.S., 2001. Post-earthquake investigation on several geosynthetic-reinforced soil retaining walls and slopes during the Ji-Ji earthquake of Taiwan. Soil dynamics and earthquake engineering 21, 297-313.

Ling, H.I., Leshchinsky, D., Perry, E.B., 1997. Seismic design and performance of geosynthetic-reinforced soil structures. Geotechnique 47 (5), 933-952.

Ling, H.I., Liu, H., Kaliakin, V.N., Leshchinsky, D., 2004. Analyzing Dynamic Behavior of Geosynthetic-Reinforced Soil Retaining Walls. Journal of Engineering Mechanics 130 (8), 911-920.

Ling, H.I., Mohri, Y., Kawabata, T., 1998. Tensile Properties of Geogrids Under Cyclic Loadings. Journal of Geotechnical and Geoenvironmental Engineering 124 (8), 782-787.

Ling, H.I., Mohri, Y., Leshchinsky, D., 2005. Large-scale shaking table tests on modular block reinforced Soil retaining walls. Journal of Geotechnical and Geoenvironmental Engineering 131 (4), 465-476.

Matsuo, O., Tsutsumi, T., Yokoyama, K., Saito, Y., 1998. Shaking table tests and analyses of geosynthetic-reinforced soil retaining walls. Geosynthetics International 5 (1-2), 97-126.

Michalowski, R.L., 1998. Limit analysis in stability calculations of reinforced soil structures. Geotextiles and Geomembranes 16 (6), 311-331.

Michalowski, R.L., You, L., 2000. Displacements of Reinforced Slopes Subjected to Seismic Loads. Journal of Geotechnical and Geoenvironmental Engineering 126 (8), 685-694.

Min, Y., Leshchinskyb, D., Ling, H.I., Kaliakin, V.N., 1995. Effects of Sustained and Repeated Tensile Loads on Geogrids Embedded in Sand. Geotechnical Testing Journal 18 (2), 204-225.

Moraci, N., Cardile, G., 2008. Pullout behaviour of different geosynthetics embedded in granular soils, 4th Asian Regional Conference on Geosynthetics, Shanghai, China, pp. 146-150.

Moraci, N., Cardile, G., 2009. Influence of cyclic tensile loading on pullout resistance of geogrids embedded in a compacted granular soil. Geotextiles and Geomembranes 27 (6), 475-487.

Moraci, N., Cardile, G., 2012. Deformative behaviour of different geogrids embedded in a granular soil under monotonic and cyclic pullout loads. Geotextiles and Geomembranes 32, 104-110.

Moraci, N., Cardile, G., Gioffrè, D., Mandaglio, M.C., Calvarano, L.S., Carbone, L., 2014. Soil Geosynthetic Interaction: Design Parameters from Experimental and Theoretical Analysis. Transportation Infrastructure Geotechnology 1, 165-227.

Moraci, N., Cardile, G., Pisano, M., 2017. Soil-geosynthetic interface behaviour in the anchorage zone [Comportamento all'interfaccia terreno-geosintetico nella zona di ancoraggio]. Rivista italiana di geotecnica 51 (1), 5-25.

Moraci, N., Recalcati, P., 2006. Factors affecting the pullout behaviour of extruded geogrids embedded in compacted granular soil. Geotextiles and Geomembranes 24 (4), 220-242.

Motta, E., 1996. Earth pressure on reinforced earth walls under general loading. Soils and Foundations 36 (4), 113-117.

Nayeri, A., Fakharian, K., 2009. Study on Pullout Behavior of Uniaxial HDPE Geogrids Under Monotonic and Cyclic Loads. International Journal of Civil Engineering 7 (4), 211-223.

Nernheim, A., 2005. Interaktionsverhalten von Geokunststoff und Erdstoff bei statischen und zyklishen Beansprungen. Ph.D. Thesis.TU Clausthal.

Newmark, N.M., 1965. Effects of earthquakes on dam and embankments. Geotechnique 15 (2), 139-160.

Nouri, H., Fakher, A., Jones, C.J.F.P., 2006. Development of Horizontal Slice Method for seismic stability analysis of reinforced slopes and walls. Geotextiles and Geomembranes 24 (3), 175-187.

Nova-Roessig, L., Sitar, N., 2006. Centrifuge Model Studies of the Seismic Response of Reinforced Soil Slopes. Journal of Geotechnical and Geoenvironmental Engineering 132 (3), 388-400.

Palmeira, E.M., 2009. Soil–geosynthetic interaction: Modelling and analysis. Geotextiles and Geomembranes 27 (5), 368-390.

Paulsen, S.B., Kramer, S.L., 2004. A predictive model for seismic displacement of reinforced slopes. Geosynthetics International 11 (6), 407-428.

Pavanello, P., Carrubba, P., Moraci, N., 2018. Dynamic friction and the seismic performance of geosynthetic interfaces. Geotextiles and Geomembranes 46, 715-725.

Rahmaninezhad, S., Han, J., Kakrasul, J., Weldu, M., 2019. Stress Distributions and Pullout Responses of Extensible and Inextensible Reinforcement in Soil Using Different Normal Loading Methods. Geotechnical Testing Journal.

Raju, D.J., Fannin, J., 1997. Monotonic and cyclic pull-out resistance of geogrids. Geotechnique 47 (2), 331-337.

Razzazan, S., Keshavarz, A., Mosallanezhad, M., 2018. Pullout behavior of polymeric strip in compacted dry granular soil under cyclic tensile load conditions. Journal of Rock Mechanics and Geotechnical Engineering 10, 968-976.

Roodi, G.H., Zornberg, J.G., 2017. Stiffness of Soil-Geosynthetic Composite under Small Displacements. II: Experimental Evaluation. Journal of Geotechnical and Geoenvironmental Engineering 143.

Sabermahani, M., Ghalandarzadeh, A., Fakher, A., 2009. Experimental study on seismic deformation modes of reinforced-soil walls. Geotextiles and Geomembranes 27 (2), 121-136.

Sieira, A.C.C.F., Gerscovich, D.M.S., Sayao, A.S.F.J., 2009. Displacement and load transfer mechanisms of geogrids under pullout condition. Geotextiles and Geomembranes 27, 241-253.

Tatsuoka, F., 2008. Geosynthetics engineering, combining two engineering disciplines, 4th Geosynthetics Asia - Special Lecture, Shanghai, Cina, pp. 1-35.

Tatsuoka, F., Koseki, J., Tateyama, M., 1995. Performance of geogrid-reinforced soil retaining walls during the Great Hanshin-Awaji Earthquake, January 17, 1995. Earthquake Geotechnical Engineering Journal, 55-62.

Tatsuoka, F., Koseki, J., Tateyama, M., 1997. Performance of reinforced soil structures during the 1995 Hyogo-ken Nanbu Earthquake. Balkema, Rotterdam, The Netherlands, pp. 973-1008.

UNI EN ISO 13286-2, 2010. Miscele non legate e legate con leganti idraulici – Parte 2: Metodi di prova per la determinazione della massa unica e del contenuto di acqua di riferimento di laboratorio – Costipamento Proctor. Ente Nazionale Italiano di Unificazione, Milano.

UNI EN ISO 14688-1, 2018. Indagini e prove geotecniche - Identificazione e classificazione dei terreni - Parte 1: Identificazione e descrizione. Ente Nazionale Italiano di Unificazione, Milano.

Vieira, C.S., Lopes, M.d.L., 2013. Effects of the loading rate and cyclic loading on the strength and deformation properties of a geosynthetic. Construction and Building Materials 49, 758-765.

Wang, Z., Jacobs, F., Ziegler, M., 2016. Experimental and DEM investigation of geogrid–soil interaction under pullout loads. Geotextiles and Geomembranes 44, 230-246.

Wartman, J., Rondinel-Oviedo, E.A., Rodriguez-Marek, A., 2006. Performance and Analyses of Mechanically Stabilized Earth Walls in the Tecomán, Mexico Earthquake. Journal of Performance of Constructed Facilities 20, 287-299.

Watanabe, K., Munaf, Y., Koseki, J., Tateyama, M., Kojima, K., 2003. Behaviors Of Several Types Of Model Retaining Walls Subjected To Irregular Excitation. Soils And Foundations 43 (5), 13-27.

White, D.M., Holtz, R.D., 1994. Performance of Geosynthetic-Reinforced Slopes and Walls During the Northridge, California Earthquake of January 17, 1994, Earth Reinforcement: Proceedings of the International Symposium on Earth Reinforcement, IS-Kyushu '96. , Fukuoka, Kyushu, Japan, pp. 965-972.

Yasuda, S., Nagase, H., Marui, H., 1992. Cyclic pull-out test of geogrids in soils, International Symposium on Earth Reinforcement Practice, Fukuoka, Japan pp. 185-190.

Zhou, J., Chen, J.-F., Xue, J.-F., Wang, J.-Q., 2012. Micro-mechanism of the interaction between sand and geogrid transverse ribs. Geosynthetics International 19 (6), 426-437.

Ziegler, M., Timmers, V., 2004. A new approach to design geogrid reinforcement, 3rd European Geosynthetics Conference, Munich, Germany.